High power Nb-doped LiFePO₄ Li-ion battery cathodes; pilot-scale synthesis and electrochemical properties

Johnson, I. D., Blagovidova, E., Dingwall, P. A., Brett, D. J. L., Shearing, P. R., & Darr, J. A. (2016). High power Nb-doped LiFePO₄ Li-ion battery cathodes; pilot-scale synthesis and electrochemical properties. *Journal of Power Sources*, *326*, 476-481. https://doi.org/10.1016/j.jpowsour.2016.06.128

Document Version:
Publisher's PDF, also known as Version of record

Queen's University Belfast - Research Portal:
Link to publication record in Queen's University Belfast Research Portal

Short communication

High power Nb-doped LiFePO$_4$ Li-ion battery cathodes; pilot-scale synthesis and electrochemical properties

Ian D. Johnson [a], Ekaterina Blagovidova [a], Paul A. Dingwall [a], Dan J.L. Brett [b], Paul R. Shearing [b], Jawwad A. Darr [a, *, 1]

[a] Department of Chemistry, University College London, London WC1H 0AJ, UK
[b] Department of Chemical Engineering, University College London, London WC1E 7JE, UK

HIGHLIGHTS

- Nb-doped LiFePO$_4$ nanoparticles (<100 nm) are synthesised *via* CHFS.
- The fructose precursor provided a continuous carbon coating.
- The doped samples display improved discharge capacities at high current rates.
- The optimal sample LiFe$_{0.99}$Nb$_{0.01}$PO$_4$ achieved 110 mA h g^{-1} at 10 C.
- Conductivity benefit of Nb confirmed by conductive carbon additive.

ARTICLE INFO

ABSTRACT

High power, phase-pure Nb-doped LiFePO$_4$ (LFP) nanoparticles are synthesised using a pilot-scale continuous hydrothermal flow synthesis process (production rate of 6 kg per day) in the range 0.01 −2.00 at% Nb with respect to total transition metal content. EDS analysis suggests that Nb is homogeneously distributed throughout the structure. The addition of fructose as a reagent in the hydrothermal flow process, followed by a post synthesis heat-treatment, affords a continuous graphitic carbon coating on the particle surfaces. Electrochemical testing reveals that cycling performance improves with increasing dopant concentration, up to a maximum of 1.0 at% Nb, for which point a specific capacity of 110 mAh g^{-1} is obtained at 10 C (6 min for the charge or discharge). This is an excellent result for a high power cathode LFP based material, particularly when considering the synthesis was performed on a large pilot-scale apparatus.

© 2016 The Authors. Published by Elsevier B.V. This is an open access article under the CC BY license (http://creativecommons.org/licenses/by/4.0/).

1. Introduction

Lithium iron phosphate (LFP, LiFePO$_4$) based cathodes for Li-ion batteries were initially developed by Goodenough and coworkers [1], and have generated interest as safer, more sustainable alternatives to current commercial Li-ion battery cathodes based on LiCoO$_2$ [2]. However, bulk LFP does not possess high electronic conductivity and high ionic diffusivity required for outstanding performance (in the ranges of 10^{-9} to 10^{-8} S cm^{-1} and 10^{-17} to 10^{-12} cm^2 s^{-1}, respectively) [3].

A number of approaches have been employed to improve the power and energy performance of pure LFP, which include coating LFP particles with conducting carbon or nano-sizing [4,5]. Furthermore, doping of metal ions (such as ions of Nb, V, or Mg) can also distort the olivine lattice, resulting in increased Li-ion transport, and furthermore generate Li$^+$ vacancies to boost Li-ion conductivity and improve high power performance [6–11]. Du and coworkers reported that an optimal dopant level of 1 at% Nb in LFP (carbon coated), gave a specific capacity of 82 mA h g^{-1} at 10 C (6 min for a charge/discharge) [12]. In contrast, Zhuang and coworkers achieved a specific capacity of 143 mA h g^{-1} at 2 C for 1 at% Nb-doped LFP [13]. The improved discharge capacity achieved by Nb-doped LFP materials could justify the incorporation of the more expensive Nb metal ion in the LFP lattice in commercial cells.

* Corresponding author. Christopher Ingold Laboratories, Department of Chemistry, University College London, 20 Gordon Street, London, WC1H 0AJ, UK.
E-mail address: j.a.darr@ucl.ac.uk (J.A. Darr).
[1] Research webpage http://www.ucl.me.uk.

Continuous hydrothermal flow synthesis (CHFS) and similar flow methods represent a relatively under-explored approach for the synthesis of Li-ion battery anodes [14–16] and cathodes [17–22]. In CHFS, a flow of supercritical water is mixed with an aqueous metal salt, which results in rapid conversion of the aqueous metal salt to form nanoparticles of metal oxide [23–25] or phosphate [22,26,27]. Furthermore, CHFS is highly scalable, allowing synthesis of nanomaterials at multi-kg per day rate [28], including vanadium-doped LFP synthesised previously by the authors [22]. Herein, the authors report the first continuous synthesis and optimisation of carbon-coated Nb-doped LFP nanoparticle cathodes using a pilot-scale CHFS process.

2. Experimental

2.1. Materials and precursors

Iron(II) sulfate, $FeSO_4 \cdot 7H_2O$ (99.5%), and lithium hydroxide, $LiOH \cdot H_2O$ (99+ %), were supplied by Fisher Scientific UK Ltd. (Loughborough, UK). Ammonium niobate(V) oxalate pentahydrate, $C_4H_4NNbO_9 \cdot 5H_2O$ (99.99%), D(−)fructose (≥99%), and phosphoric acid (85 wt%) were supplied by Sigma-Aldrich Ltd. (Dorset, UK). Deionised water was used throughout (>10 MΩ cm^{-1}). All starting solutions, precursors and deionised water were degassed with pure nitrogen gas prior to reaction.

2.2. Continuous hydrothermal flow syntheses

The synthesis was conducted using a pilot-scale CHFS reactor, a detailed description of which can be found elsewhere [28,29]. In the process, an aqueous precursor solution containing an appropriate mixture of ammonium niobate and iron(II) sulfate (total concentration 0.25 M, Table S1), fructose (0.65 M), and phosphoric acid (0.375 M) was pumped into a ¼ inch Swagelok™ tee-piece to meet a second pumped flow of 0.8625 M lithium hydroxide solution (each at a flow rate of 200 mL min^{-1}). This combined flow of precursors was then brought into contact with a stream (400 mL min^{-1}) of supercritical D.I. water at 450 °C and 240 bar in a ¾ inch confined jet mixer. A schematic of the synthesis process and the confined jet mixer are shown in Fig. S1 and Fig. S2, respectively. The combined concentrations of iron and niobium ions (total 0.25 M), phosphoric acid, lithium hydroxide and fructose were kept constant at the ratio 1.00: 1.50: 3.45: 2.60. Further details are included in the Supporting Information.

2.3. Instrumentation

Powder XRD data were obtained on a (STOE StadiP) diffractometer using Mo-Kα radiation (λ = 0.71069 nm) in the 2θ range of 2–40°, with a step size of 0.5° and a step time of 10 s. CHN analysis was performed on a horizontal load CHN analyser (Exeter Analytical EA-440 instrument). A Renishaw inVia™ Raman Microscope with a 785 nm diode laser was used to obtain Raman spectra. The laser power was set to 10% of full power for all samples. Scans were collected in the range 200–2000 cm^{-1} with a total scan time of 2 min. Energy dispersive X-ray spectroscopy (EDS) analysis was performed using an Oxford Instruments X-MaxN 80-T Silicon Drift Detector fitted to a Jeol JEM-1010 transmission electron microscope. TEM samples were prepared by pipetting drops of ethanol (99.9%, Sigma Aldrich, Dorset UK) containing ultrasonically dispersed particles on to copper film grids (300 mesh - Agar Scientific, UK). Field emission scanning electron microscopy (FE-SEM) images were obtained using a JEOL JSM-6700F microscope.

2.4. Preparation of printed electrodes and half cells and electrochemical testing

Cathode inks were prepared by thoroughly mixing the heat-treated samples, conductive agent (carbon black, Super P™, Alfa Aesar, Heysham, UK), and PVDF (polyvinylidene fluoride, PI-KEM, Staffordshire, UK) in an NMP solvent (N-methyl-2-pyrrolidone solvent, Sigma Aldrich, St Louis, USA). Two electrodes were prepared; set one had a wt% ratio of 80:10:10 S:C:B (sample: added carbon: binder), whilst set two contained a higher added carbon loading of 75:15:10 S:C:B. The preparation of the electrodes, coin cells and electrochemical tests are described in the Supporting Information.

2.5. Results and discussion

LFNP nanoparticles were synthesised using CHFS as described in the experimental section. For samples named LFNP(x), x is the nominal Nb at% present in the precursor solution, relative to total transition metal content. The samples were heat-treated to further graphitise the surface carbon coatings, giving the corresponding ΔLFNP(x) compounds.

Powder XRD patterns of heat-treated samples all displayed the pure $LiFePO_4$ olivine structure (Fig. 1), with no significant peak shift (within errors) between samples. This was in contrast to the report of Du and co-workers, where the addition of the Nb dopant was found to increase the (1 0 1) interplanar distance [12]. EDS analysis of sample ΔLFNP(2.0) showed a uniform dispersion of Nb within
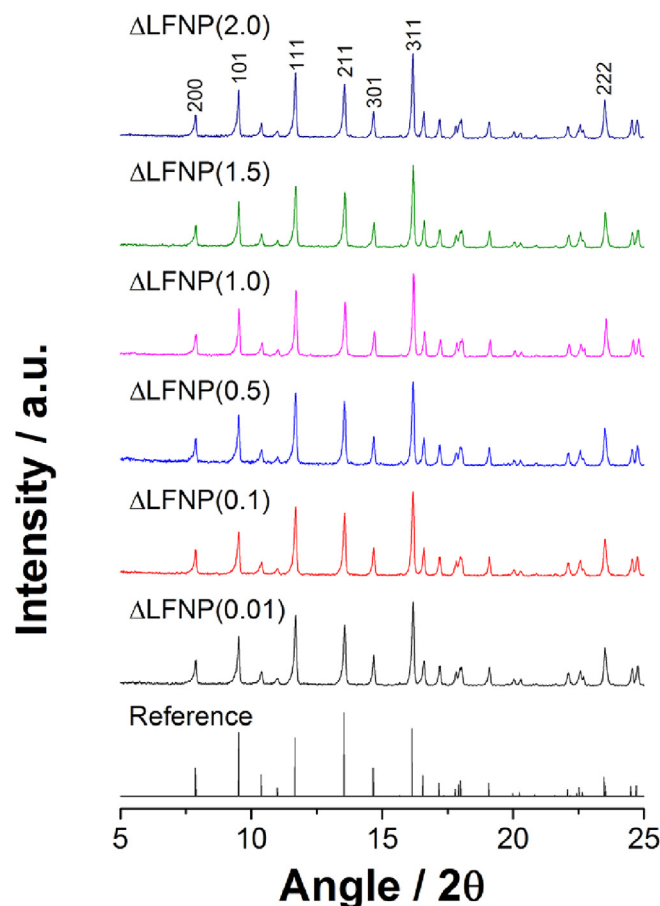

Fig. 1. Normalised powder XRD patterns of the heat-treated (Δ) Nb-doped samples with the JCPDS reference pattern for $LiFePO_4$ (JCPDS 00-040-1499).
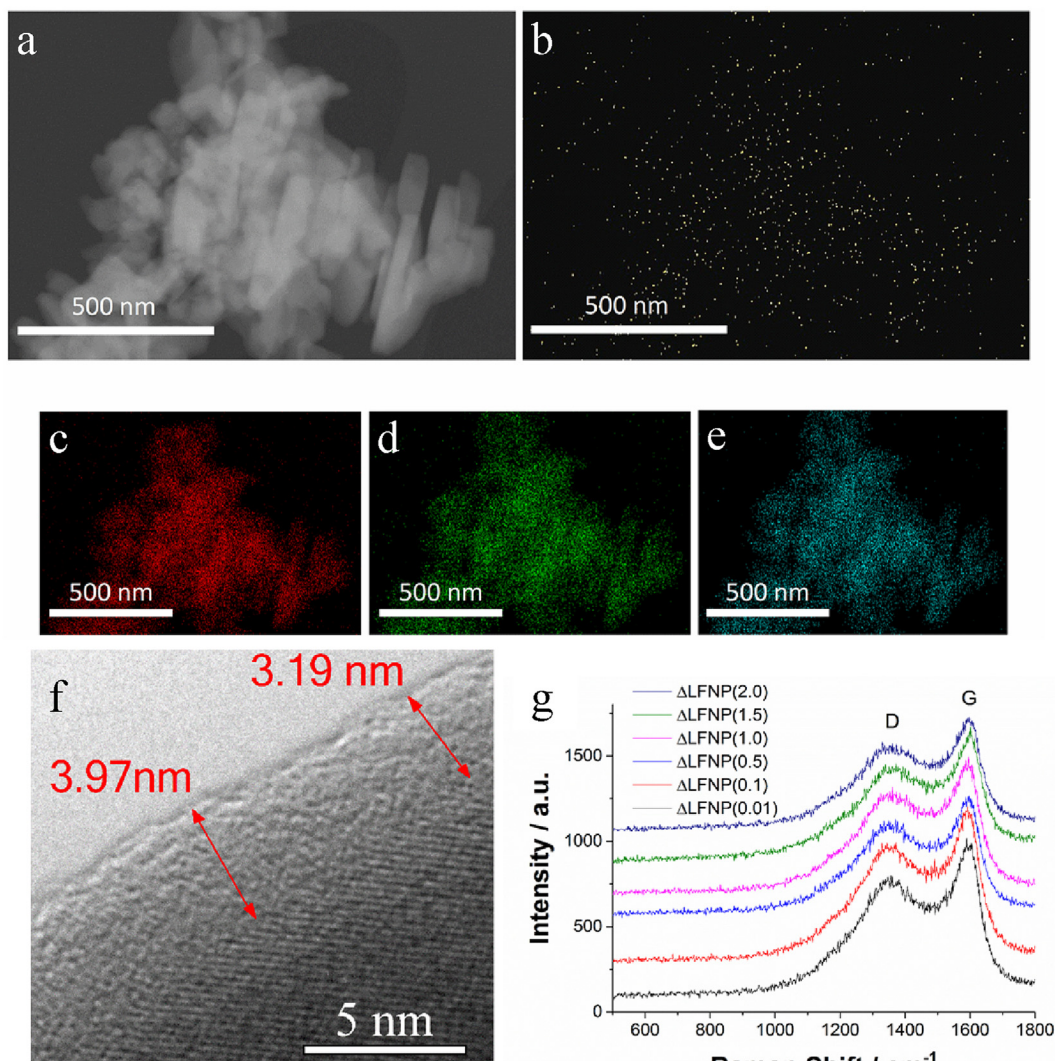
Fig. 2. EDS imaging of sample LFNP(2.0) showing a) the darkfield image, b) the Nb Kα signals, c) the Fe Kα signals, d) the O Kα signals and e) the P Kα signals; f) A TEM micrograph of sample ΔLFNP(1.0); g) Raman spectra of the heat-treated samples showing the graphitic D and G bands.

the particles (Fig. 2a–e). This implied Nb was homogeneously doped within the olivine structure, although techniques such as XAS could further confirm this in future work.

FE-SEM analysis indicated the particle size and shape varied significantly within samples (Fig. S3), which formed agglomerated networks of <100 nm semi-spherical crystallites and larger
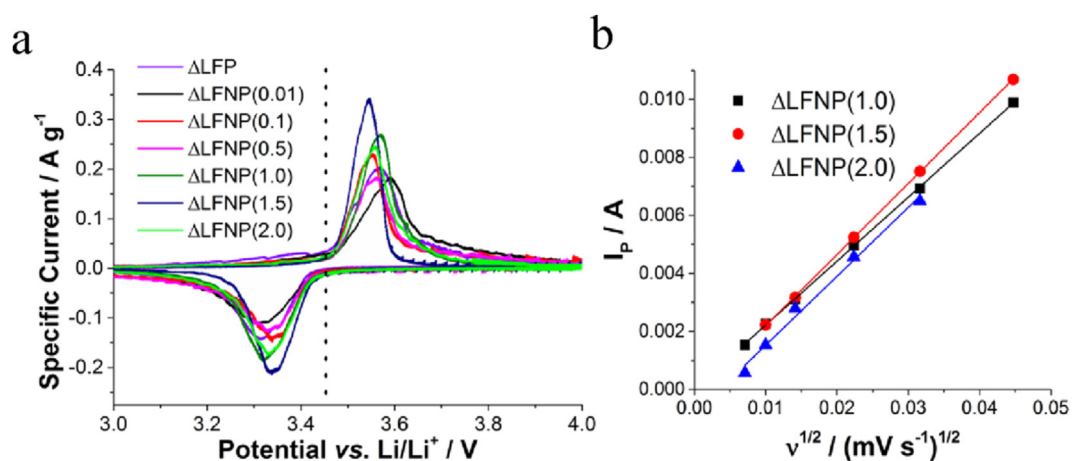

Fig. 3. a) Cyclic voltammograms at 0.05 mV s^{-1} scan rate for all heat-treated samples, including a pure LFP sample from previous work; b) linear fits obtained from the cyclic voltammetry data of peak current (I_p), versus the square root of the scan rate ($\nu^{1/2}$) for samples ΔLFNP(1.0), ΔLFNP(1.5), and ΔLFNP(2.0) (active:carbon:binder wt% ratio 80:10:10).
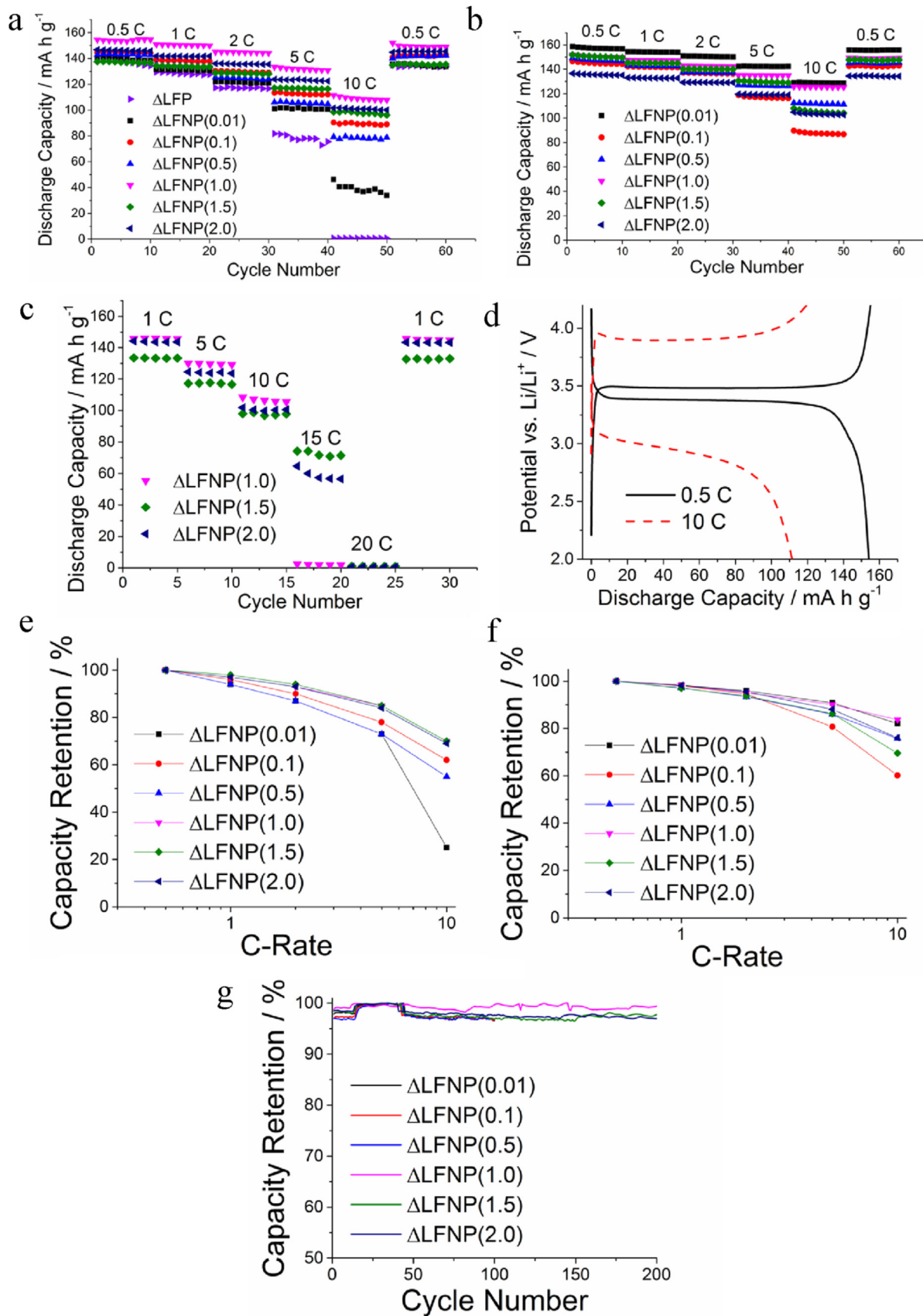
Fig. 4. Variable C-rate tests (at C-rates shown) for all electrodes with S:C:B wt% ratios of a) 80:10:10 (including a pure LFP sample from previous work) and b) 75:15:10. c) Tests of ΔLFNP(1.0), ΔLFNP(1.5), and ΔLFNP(2.0) at higher C-rates (solid active:carbon:binder {S:C:B} wt% ratio of 80:10:10). d) A voltage vs. capacity plot of ΔLFNP(1.0) (80:10:10) at 0.5 C and 10 C. Capacity retention test data at for all doped LFP samples with S:C:B wt% ratios of: e) 80:10:10; f) 75:15:10. The original capacity is the discharge capacity of each cell at 0.5 C. g) Capacity retention at a charge and discharge rate of 1 C of set 1 samples ΔLFNP(0.01), ΔLFNP(0.1), and ΔLFNP(0.5) for 100 cycles and samples ΔLFNP(1.0), ΔLFNP(1.5), and ΔLFNP(2.0) for 200 cycles. The capacity retention was relative to the highest capacity observed during these cycles.

rhombic-morphology particles, similar to LFP and doped LFP synthesised *via* CHFS previously [22]. Therefore, Nb-doping did not significantly alter crystallite size or morphology.

The carbon content of the heat-treated samples varied in the range 2.5–7.3 wt% (Table S1). TEM micrographs of the heat-treated compound ΔLFNP(1.0), showed the carbon formed a continuous coating approximately 3.5 nm thick (Fig. 2f). Raman spectroscopy analysis of the heat-treated samples, showed a D-band (1350 cm^{-1}) and G-band (1600 cm^{-1}, Fig. 2g), where the intensity ratio I_D/I_G was similar between samples (0.7–0.8, Table S2). No peak indicative of the PO_4 group could be observed, which in combination with the TEM, suggested the graphitic carbon layer effectively covered the surface of the particles.

Cyclic voltammetry experiments confirmed the presence of the Fe^{2+}/Fe^{3+} redox couple at 3.45 V, indicated by the dotted line (Fig. 3a) with no additional redox activity observed due to the Nb dopant. The peak current generally increased with Nb content up to 1.5 at%, and thereafter, it decreased for 2.0 at% Nb-doping. This behaviour clearly demonstrates the addition of Nb, generally improved lithiation and delithiation kinetics in the samples. A pure ΔLFP electrode from previous work by the authors, is included as reference; while the peak current achieved by this sample is higher than ΔLFNP(0.01)-ΔLFNP(0.5), the carbon content of the ΔLFP sample was much higher (9.1 wt% vs. 2.5–7.3 wt%). To investigate this further, a qualitative Li-ion diffusion coefficient analysis was conducted using the Randles-Sevcik equation (Equation (1), Supporting Information) [30,31]. The diffusion coefficients obtained are dependent upon many different properties of the cell (such as mass loading and proportion of carbon and binder in the electrode), so are used only for comparison with electrodes within this study (which were prepared and assembled identically).

$$I_p = \left(2.69 \times 10^5\right) C.A.D^{1/2} n^{3/2} \nu^{1/2} \tag{1}$$

The calculated diffusion coefficients were very similar, with values of 2.0×10^{-10}, 2.2×10^{-10} and 1.9×10^{-10} cm^2 s^{-1} for samples ΔLFNP(1.0), ΔLFNP(1.5) and ΔLFNP(2.0), respectively. This shows an increase compared to pure LFP (1.0×10^{-10} cm^2 s^{-1}) previously reported by the authors, and suggested that Nb doping beyond 1 at% added little benefit to performance [22].

Constant current tests on the same cells, showed that the rate capability of samples increased with increasing Nb content (Fig. 4a,e), especially compared to the undoped ΔLFP sample, proving that incorporation of even a small proportion of Nb has a much greater effect on performance than any dopants present from precursor impurities [22]. The best performing sample ΔLFNP(1.0) displayed a capacity of 110 mA h g^{-1} at 10 C, which surpasses capacities obtained for pure LFP materials made *via* continuous hydrothermal methods. Aimable et al. achieved 75 mA h g^{-1} at 0.1 C [32] and Kim et al. reported a capacity of 88 mA h g^{-1} at 10 C [19]. Thus, the Nb-doped LFP reported herein offers a clear high power performance advantage over the undoped material.

Electrodes with higher added carbon content (S:C:B wt% ratio 75:15:10) were also examined. Much smaller variation in cell performance was observed, regardless of Nb content (Fig. 4b,f). In this case, the ΔLFNP(0.01) cell performed best, which suggested that the Nb dopant enhanced the electrical conductivity of LFP, and the effect is reduced with a higher proportion of conductive carbon in the electrode. This is consistent with conductivity analysis performed previously by other researchers [13,33].

The three highest performing electrodes (80:10:10 wt% S:C:B ratio) were ΔLFNP(1.0), ΔLFNP(1.5), and ΔLFNP(2.0), which were subjected to further constant rate tests using high C-rates (Fig. 4c). Beyond 10 C, most electrodes tended not to provide any appreciable capacity as the overpotential required to charge the cells often moved beyond the operating voltage window (Fig. 4d). All three electrodes recovered full capacity after cycling at 20 C. Comparing the capacity retention of all samples as a function of C-rate also indicated the limiting conductivity benefit of the Nb dopant up to 1 at% Nb (Fig. 4e), where ΔLFNP(1.0), ΔLFNP(1.5), and ΔLFNP(2.0) displayed an equal capacity retention of ca. 70% (of the original value at C/2) at 10 C (Fig. 4e). Excellent capacity retention (range 96–98%) was also observed in long term stability testing at a 1 C charge/discharge rate (range of 100–200 cycles) for the same cells (Fig. 4g).

3. Conclusions

The synthesis of nano-sized, carbon-coated, Nb-doped LFP was achieved at a production rate of *ca.* 0.25 kg h^{-1} using a pilot-scale CHFS process. Elemental mapping suggested that Nb was evenly distributed throughout the LFP particles. Electrochemical testing showed improved performance with increasing Nb content, where the 1 at% Nb-doped sample achieved a specific discharge capacity of 110 mAh g^{-1} at 10 C, a substantial improvement on pure LFP. Increasing dopant levels above 1 at% Nb led to no additional performance gains. Experiments with higher levels of conductive carbon additive suggested that Nb-doping increased the electrical conductivity of the material. This high performance is especially significant given the high production rate herein, and therefore represents evidence that continuous hydrothermal flow reactors could produce high-quality battery electrodes at scale.

Appendix A. Supplementary data

Supplementary data related to this article can be found at http://dx.doi.org/10.1016/j.jpowsour.2016.06.128.

Conflict of interest

The authors declare no competing financial interests.

References

[1] A.K. Padhi, K.S. Nanjundaswamy, J.B. Goodenough, J. Electrochem. Soc. 144 (1997) 1188–1194.
[2] M.S. Whittingham, Chem. Rev. 104 (2004) 4271–4301.
[3] O.K. Park, Y. Cho, S. Lee, H.-C. Yoo, H.-K. Song, J. Cho, Energ. Environ. Sci. 4 (2011) 1621–1633.
[4] M. Gaberscek, R. Dominko, J. Jamnik, Electrochem. Commun. 9 (2007) 2778–2783.
[5] Y. Wang, Y. Wang, E. Hosono, K. Wang, H. Zhou, Angew. Chem. 47 (2008) 7461–7465.
[6] S.-Y. Chung, J.T. Bloking, Y.-M. Chiang, Nat. Mater. 1 (2002) 123–128.
[7] N. Meethong, Y.-H. Kao, S. Speakman, Y.-M. Chiang, Adv. Funct. Mater. 19 (2009) 1060–1070.
[8] J. Hong, C.S. Wang, X. Chen, S. Upreti, M.S. Whittingham, Electrochem. Solid-State Lett. 12 (2009) A33–A38.
[9] K.L. Harrison, C.A. Bridges, M.P. Paranthaman, C.U. Segre, J. Katsoudas, V.A. Maroni, J.C. Idrobo, J.B. Goodenough, A. Manthiram, Chem. Mater. 25 (2013) 768–781.
[10] K. Hoang, M.D. Johannes, J. Power Sources 206 (2012) 274–281.
[11] H. Liu, C. Li, Q. Cao, Y. Wu, R. Holze, J. Solid State Electrochem. 12 (2008) 1017–1020.
[12] Z.P. Ma, G.J. Shao, G.L. Wang, Y. Zhang, J.P. Du, J. Solid State Chem. 210 (2014) 232–237.

[13] D.G. Zhuang, X.B. Zhao, J. Xie, J. Tu, T.J. Zhu, G.S. Cao, Acta Phys.-Chim. Sin. 22 (2006) 840–844.
[14] M. Lübke, I. Johnson, N.M. Makwana, D. Brett, P. Shearing, Z. Liu, J.A. Darr, J. Power Sources 294 (2015) 94–102.
[15] M. Lübke, N.M. Makwana, R. Gruar, C. Tighe, D. Brett, P. Shearing, Z. Liu, J.A. Darr, J. Power Sources 291 (2015) 102–107.
[16] M. Lubke, J. Shin, P. Marchand, D. Brett, P. Shearing, Z. Liu, J.A. Darr, J. Mater Chem. A 3 (2015) 22908–22914.
[17] C. Xu, J. Lee, A.S. Teja, J. Supercrit. Fluid 44 (2008) 92–97.
[18] A. Aimable, H. Muhr, C. Gentric, F. Bernard, F. Le Cras, D. Aymes, Powder Technol. 190 (2009) 99–106.
[19] S.A. Hong, S.J. Kim, J. Kim, B.G. Lee, K.Y. Chung, Y.W. Lee, Chem. Eng. J. 198 (2012) 318–326.
[20] S.A. Hong, A. Nugroho, S.J. Kim, J. Kim, K.Y. Chung, B.W. Cho, J.W. Kang, Res. Chem. Intermed. 37 (2011) 429–440.
[21] S.A. Hong, S.J. Kim, J. Kim, K.Y. Chung, B.W. Cho, J.W. Kang, J. Supercrit. Fluid 55 (2011) 1027–1037.
[22] I.D. Johnson, M. Lübke, O.Y. Wu, N.M. Makwana, G.J. Smales, H.U. Islam, R.Y. Dedigama, R.I. Gruar, C.J. Tighe, D.O. Scanlon, F. Corà, D.J.L. Brett, P.R. Shearing, J.A. Darr, J. Power Sources 302 (2016) 410–418.
[23] J.A. Darr, M. Poliakoff, Chem. Rev. 99 (1999) 495–541.
[24] J.B. Goodall, D. Illsley, R. Lines, N.M. Makwana, J.A. Darr, ACS Comb. Sci. 17 (2015) 100–112.
[25] S. Elouali, L.G. Bloor, R. Binions, I.P. Parkin, C.J. Carmalt, J.A. Darr, Langmuir 28 (2012) 1879–1885.
[26] A.A. Chaudhry, J. Goodall, M. Vickers, J.K. Cockcroft, I. Rehman, J.C. Knowles, J.A. Darr, J. Mater. Chem. 18 (2008) 5900–5908.
[27] A.A. Chaudhry, J.C. Knowles, I. Rehman, J.A. Darr, J. Biomater. Appl. 28 (2013) 448–461.
[28] R.I. Gruar, C.J. Tighe, J.A. Darr, Ind. Eng. Chem. Res. 52 (2013) 5270–5281.
[29] C.J. Tighe, R.I. Gruar, C.Y. Ma, T. Mahmud, X.Z. Wang, J.A. Darr, J. Supercrit. Fluid 62 (2012) 165–172.
[30] N. Tanaka, R. Tamamushi, Electrochim. Acta 9 (1964) 963–989.
[31] S. Yang, X. Zhou, J. Zhang, Z. Liu, J. Mater. Chem. 20 (2010) 8086–8091.
[32] A. Aimable, D. Aymes, F. Bernard, F. Le Cras, Solid State Ionics 180 (2009) 861–866.
[33] S.Y. Chung, J.T. Bloking, Y.M. Chiang, Nat. Mater. 1 (2002) 123–128.